Anisotropic diffusion in *Cyphochilus* white beetle scales

Seung Ho Lee,[1] Sang M. Han,[1] Sang Eon Han[1,*]
[1]Department of Chemical and Biological Engineering, 1 University of New Mexico, Albuquerque, NM 87131, USA
[*]Email: sehan@unm.edu

Abstract:
Cyphochilus white beetles possess an exceptional ability to scatter visible light from their scales, which have anisotropic nanofibrillar network structures. We discover a striking effect that diffusely incident light on the beetle scales is preferentially channeled sideways and scattered backward on the average after traversing a vertical distance corresponding to only two scattering events. For normally incident light, the scattering is only slightly forward, resulting in close proximity between two optical characteristic lengths: scattering mean free path (1.78 μm) and *effective* transport mean free path (1.85 μm). We have used *effective* transport mean free path to properly describe the scattering strength in anisotropic random media. For improved description of light scattering in beetle scales, we apply complete solutions to the anisotropic diffusion equation, where the solution approach made use of optical boundary layer theory. Our method enables highly accurate determination of mean free paths and extrapolation length in the white beetle scales.

I. INTRODUCTION

Nature, through hundreds of millions of years of adaptive evolution, offers extraordinary physical properties in light scattering,[1] surface hydrophobicity,[2] and mechanical strength at light weight,[3] using intricate micro and nanostructures. These structures often exploit intriguing physical principles that are not yet fully understood. In this work, we focus on *Cyphochilus* white beetles that embody such extraordinary properties. The scales of these beetles display strong broadband light scattering power[4-6] that is an order of magnitude greater than common white papers.[4,6] To date, many scientific investigations[4-8] have been made to extract optical characteristics of the scales and to determine whether the nanostructures in the scales are fully evolved for maximum light scattering. Contrary to the long-time belief that the scale nanostructures are fully optimized for high-level scattering,[4-6] recent studies contend that further optimization would be necessary for even stronger scattering.[9-11]

The nanostructures in *Cyphochilus* white beetle scales are highly anisotropic. A recent numerical study has demonstrated the important role of anisotropy expressed in scatterer shape and orientation.[11] Despite this extensive work, a question still remains as to *how* the structural anisotropy in *Cyphochilus* white beetle scales maximizes light scattering and shapes light propagation. To address this question, in this work, we establish methods to accurately characterize optical scattering in such anisotropic media. The accurate optical characterization reveals *how* the structural anisotropy in *Cyphochilus* white beetle scales achieves the strong scattering. Specifically, we discover that the anisotropic structure gives rise to a striking optical characteristic, where the diffusely incident light is preferentially channeled sideways and scattered backward, on the average, after traversing a vertical distance corresponding to only two scattering events.

The internal structure of *Cyphochilus* scales holds the key to the strong broadband light scattering. Each scale is shaped like an elliptical disk with approximately 200 μm × 60 μm lateral dimensions and 7 μm thickness.[5-7] These scales cover the black exocuticle of the beetle in a close-packed, disordered manner with a partial overlap between adjacent scales. Each scale has an internal structure that is a continuous network of randomly distributed fibrils made of chitin. Chitin is a biopolymer that has a relatively low refractive index of ~1.56.[12,13] The fibrils are highly aligned in lateral directions with an average fibril diameter of ~250 nm,[4,6,7,14] and the anisotropic fibrillar network is encapsulated by a 250 to 550-nm-thick solid shell.[5,6,14]

Previous studies[4,5,8] applied the diffusion theory to estimate the transport mean free path of white beetle scales. Transport mean free path (l^*) is defined as a length that light travels before its propagation direction is randomized. Burresi *et al.* estimated that $l^* = 1.47$ μm, using the isotropic diffusion equation.[4] In anisotropic media such as white beetle scales, however, l^* takes a tensorial form L^*_{ij}. Recognizing that the scale structure is highly anisotropic, Cortese *et al.* measured the transport mean free path tensor and obtained an optical anisotropy (OA) as large as 0.71, at a region of average thickness, where OA is defined as $(L^*_{xx} - L^*_{zz}) / L^*_{xx}$ with $L^*_{xx} \cong L^*_{yy}$ and the *z* axis being in the scale thickness direction.[5] In subsequent studies by Wilts *et al.*[6] and Jacucci *et al.*[8], OA was determined to be 0.52 and 0.27, respectively. The large disagreement in OA between the studies in refs [5,6,8] indicates that approximations made in a number of previous studies[4,5,8] may lead to significant errors. First, ref [5] used a transmittance expression for the isotropic diffusion equation to determine L^*_{zz}, as ref [4] used it to obtain l^*. Second, refs [4,5,8] assumed that light in the scale is internally reflected exactly at the boundary instead of a region near the boundary[16]. Errors resulting from this assumption can be particularly significant when L^*_{ij} is extracted from coherent backscattering experiment, as in ref [8], where the signal is mostly from the light that does not penetrate deep into the structure.

In order to address these potential errors, we took the following approach to describe optical

scattering in *Cyphochilus* scales with improved accuracy. Regarding the first assumption, we made a correction to the anisotropic diffusion equation and derived an expression for transmittance containing anisotropy tensor K_{ij},[15] which has been ignored in other studies. An important implication of K_{ij} is that the conventional physical meaning of transport mean free path for *z* direction must be expressed by a product of L^*_{zz} and K_{zz}, and not by L^*_{zz} alone. Regarding the second assumption, we have shown that internal reflection in highly scattering dense media does not occur exactly at the boundary but through a finite region near the boundary defined as optical boundary layer.[16] This optical boundary layer approximation showed that assuming internal reflections at the boundary can lead to a significant error in the calculated transport mean free path.

For improved description of anisotropy and internal reflection, we consider the anisotropy tensor and the optical boundary layer to determine L^*_{zz} and K_{zz} for *Cyphochilus* white beetle scales. For accurate characterization of optical scattering, we perform calculations based on high-resolution X-ray images of the scale produced by Wilts *et al*.[6] Our work improves the accuracy of transport parameters in *Cyphochilus* scales with a discovery that the direction of light propagation becomes completely randomized over the vertical distance corresponding to only two scattering events. This randomized propagation around fibrils within the surrounding anisotropic fibrillar network leads to preferential and effective channeling of light in lateral directions. This extraordinary light scattering has not been observed in other optical materials.

II. STRUCTURAL CHARCTERIZATION

Structural characteristics of *Cyphochilus* white beetle scales can be captured by typical descriptors, such as structural correlation, fill fraction, and anisotropy. We extract these descriptors from two-point probability function (S_2) based on a 3D image of the scale. The image is constructed from a video of 491 2D X-ray tomography images scanned in the thickness direction in ref [6]. From the 2D images, we select 362 *xy*-planes evenly spaced in *z*-direction along the scale thickness, occupying a 6.86 μm × 6.86 μm × 5.16 μm volume near the center of the scale. This volume is representative of the scale's core, and excludes regions near the outer shell of the scale where fill fraction changes rapidly (~0.5 μm from the top and bottom interfaces between the fibrillar network and the shell). We make use of the 3D image to calculate S_2.:

$$S_2(\boldsymbol{r}) = \int I(\boldsymbol{r}')I(\boldsymbol{r}'-\boldsymbol{r})d\boldsymbol{r}' \quad , \tag{1}$$

where $\boldsymbol{r}$ and $\boldsymbol{r}'$ are position vectors, and $I = 0$ and 1 for void and solid phase, respectively. One of the principal axes is in the *z*-direction. In Fig. 1(a), $S_2(\boldsymbol{r})$ in the *xy*-planes shows a near circular spot with rotational symmetry, indicating that the structure is isotropic in the planes. In contrast, $S_2(\boldsymbol{r})$ in other planes are not rotationally symmetric. Figure 1(b) shows $S_2(\boldsymbol{r})$ in the *xz*-planes, where the oblong bright spot indicates that the structure is strongly anisotropic.

From Figs. 1(a) and (b), we extract $S_2(r)$ where $r = x, y, z$ and display the results in Fig. 1(c). Due to the isotropy in *xy*-planes, $S_2(x)$ and $S_2(y)$ are almost indistinguishable from each other. $S_2(\boldsymbol{r})$ satisfies the conditions that $S_2(0) = f$ and $\lim_{r\to\infty} S_2(r) = f^2$ where *f* is the solid fill fraction.[17] *Applying these conditions, we determine that f = 0.315, which is in agreement with ref [9].* A modeling work showed that optical scattering is maximized in fibrillar anisotropic structures at $f \sim 0.3 - 0.4$.[10,11] However, our calculated fill fraction disagrees with the work of Wilts *et al.* who measured $f = 0.45$ from the same structure.[6] We note that this fill fraction $f = 0.45$ is inconsistent with their calculated $S_2(0) = 0.27$, which should have been same as $f = 0.45$. Our calculated range of fill fractions contrasts even more with the work by Vukusic *et al.*, who have obtained $f \sim 0.7$ [7] and refined it later as $f = 0.61$.[4]

The exact reasons for the disagreement in the *f* values among these previous publications and our

measurement are difficult to determine. However, we expect a high level of accuracy in f calculated from the high-resolution, X-ray tomography images in ref [6]. Thus, we deduce that the very high values of $f = 0.61 - 0.7$ [4,7] are strongly suspect. The beetle scale's fill fraction is also heterogeneous, showing almost uniform fill fraction near the core but rapidly increasing near the shell. While it may not be easy to discern this heterogeneity in fill fraction in the *xz*- or *yz*-plane images [*e.g.*, Figs. 1(f) and (g)], the image of an *xy*-plane at the core [Fig. 1(d)] clearly shows a smaller fill fraction than that near the shell [Fig. 1(e)]. Void and solid phases appear black and white, respectively, in Figs. 1 (d), (e), and (g). Thus, the calculated fill fraction depends on the location and size of the volume used for averaging. Consistent with this heterogeneity, the $f = 0.315$, which we have determined from images around the center plane excluding those near the top and bottom of the scale, is smaller than $f = 0.45$ reported in ref [6].

To independently confirm the validity of our measured fill fractions, we cut a *Cyphochilus* scale by a focused ion beam (FEI Quanta 3D) and obtained electron micrographs. Unlike in ref [9], we observe no deformation during the ion beam milling as in ref [4]. The image in Fig. 1(f) is taken on an *xz* cutting plane, showing structural anisotropy. For the image in Fig. 1(f), the flat regions, which are the exposed sections of the fibrils by the beam cutting, are clearly distinguished from the other regions by image contrast. To clearly show the fibril surfaces exposed by the cutting, we show a black-and-white version of the image in Fig. 1(g). From the fibrillar network regions clearly separated from the shell in this image, we find that $f = 0.32$ which is consistent with both ref [9] and our measurements based on the high-resolution images in ref [6]. This fill fraction is evidence that white beetle scales achieve a high level of scattering from a relatively sparse medium.

III. OPTICAL CHARCTERIZATION

Based on our structural analysis shown in Fig. 1, we define our simulation volume. In Fig. 1(c), we see that the correlation in the x and y directions attenuates over ~0.5 μm or less. This suggests that an *xy*-plane of the *Cyphochilus* scale with x and y dimensions much greater than ~0.5 μm would well represent its overall structure in the plane. For our optical simulations, we carve out 1.81 μm × 2.94 μm *xy* dimensions from our 3D X-ray tomography construct (6.86 μm × 6.86 μm × 5.16 μm) based on ref [6]. For the z dimension, the minimum length is yet to be determined for the simulation volume to properly represent the scattering properties of a *Cyphochilus* scale. In Fig. 1(c), the z-direction correlation also attenuates over ~0.5 μm, and the previous studies[4,5,8] report that the transport mean free path in the z-direction is approximately 1 – 1.5 μm. Based on these results, one may expect the z-dimension of the simulation volume to be much greater than 1 – 1.5 μm.[18,19] Despite this expectation, we will show later in this section that the diffusion approximation holds true for thicknesses even below the transport mean free path in the z-direction.

To determine the z-dimension of simulation volume that accurately represents the optical properties of the beetle scale, we compartmentalize the 3D tomography construct (6.86 μm × 6.86 μm × 5.16 μm) with simulation volumes whose *xy* dimensions are 1.81 μm × 2.94 μm and z-dimensions are 0.39, 1.08, 2.12, 3.16, and 4.20 μm. Once the z-dimension is chosen from this range (0.39 to 4.20 μm), we choose the lateral mid-section of the scale, and the simulation volume is translated vertically from top to bottom of the lateral mid-section of the 3D X-ray tomography construct. While the simulation volume is vertically translated, we select the volumes where $f = 0.315$ and use them for optical calculations. This approach prevents large fluctuations in f that may result from small simulation volumes.

The simulation wavelength should not be too small in comparison to the *xy* dimensions of the simulation volumes (1.81 μm × 2.94 μm) to ensure sufficient accuracy in optical calculations. In

previous studies,[4,6] the reflectance spectrum of a *Cyphochilus* scale, including the shell, was found to be almost constant from 0.45 to 0.85 μm wavelength range, whereas the reflectance spectrum of the scale core monotonically decreases in the wavelength range.[6,9] For due comparison with the previous studies, while maximizing the accuracy of our simulations, we chose a wavelength of 0.9 μm.

Scattering / transport mean free paths of random media can be calculated based on the mean field theory.[20] In the theory, one typically considers a scattering unit embedded in a homogeneous material to which an effective refractive index corresponding to the entire scattering media is assigned.[21] The scattering properties of the unit in the effective medium are then used to calculate scattering / transport mean free paths. In general, the mean field theory is highly accurate in calculating scattering properties of optically dense media. For example, transport mean free paths obtained by the mean field theory agreed well with experiments for photonic glasses.[22] For the fibrillar network structures found in the interior of the beetle scale, however, it is not intuitively easy to define a scattering unit. Thus, instead of defining a scattering unit, we obtain transport parameters by embedding simulation volumes within the effective medium. Specifically, the simulation volumes are assumed to be periodic in the *xy*-plane and are bounded by the effective medium in the *z*-direction. The refractive index of the effective medium is based on the Maxwell-Garnett theory.[23] We calculate transmittance of the simulation volumes of varying thicknesses embedded in the effective medium, and extract scattering / transport mean free paths from the transmittance.

The *zz*-component of the scattering mean free path tensor L_{zz} is calculated from $T_b(\hat{z}) = \exp(-L/L_{zz})$ where T_b is the ballistic transmittance, and L is the film thickness. Specifically, we plot $\log(1/T_b)$ vs. L and perform linear regression on the plot as shown in Fig. 2(a). L_{zz} is determined as 1.78 μm from the slope of the plot with a coefficient of determination $R^2 = 0.9920$. To find L^*_{zz} and the anisotropy tensor component K_{zz}, we use the expression for total transmittance T that derived[15] for anisotropic media:

$$T = \frac{[K_{zz} + z_e] - [K_{zz} - z_e]\exp(-L / L_{zz})}{L / L^*_{zz} + 2z_e}, \tag{2}$$

where z_e is the extrapolation length ratio. Note that, for isotropic media, K_{zz} is equal to 1 and Eq. (2) is reduced to the popular expression given in ref [24]. Equation (2) can be cast into a linear form

$$y_1 = \frac{1}{L^*_{zz}} L, \tag{3}$$

where

$$y_1 = -2z_e + K_{zz}\frac{1-\exp(-L / L_{zz})}{T} + z_e\frac{1+\exp(-L / L_{zz})}{T}. \tag{4}$$

As our first approximation, we set z_e to be 2/3 based on the diffusion theory for isotropic random media with an internal reflectance $R_i = 0$ because the simulation volume is embedded in its effective medium.[25] This approximation is valid in principle for weakly scattering isotropic media, but its accuracy becomes problematic for our strongly scattering anisotropic media.[16,26] L^*_{zz} and K_{zz} are obtained from a linear fit of the calculated transmittance to Eq. (3). L^*_{zz} is obtained from the slope, and K_{zz} is determined as the value that minimizes the root mean square error of the fit: $L^*_{zz} = 1.54$ μm and $K_{zz} = 1.2$ with $R^2 = 0.9865$ (see Table 1).

Table 1. Comparison of transport parameters obtained by conventional boundary condition and optical boundary layer theory.

Boundary Condition	z_e	L^*_{zz} (μm)	K_{zz}	L^*_{zz}' (μm)	R^2
Conventional	0.667	1.54	1.2	1.86	0.9865
Optical Boundary Layer Theory	0.519	2.05	0.9	1.85	0.9917

To improve the accuracy of L^*_{zz} and K_{zz} resulting from the above approximation, we use the optical boundary layer theory that we developed.[16] For strongly-scattering optically-dense media, internal reflection happens in an interior region near the interface, and not at the interface. Using the theory in ref [16], we calculate the internal reflectance in an optical boundary layer and obtain z_e from the accurately calculated internal reflectance. Specifically, z_e is calculated by

$$z_e = z_{e0} - \frac{a}{L_{zz}^*} = \frac{2}{3}\frac{1+R_{BL,2}}{1-R_{BL,1}} - \frac{a}{L_{zz}^*}, \tag{5}$$

where a is the optical boundary layer thickness, and $R_{BL,n}$, defined in ref [16], is the nth moment of internal reflectance from the boundary layer. Note that $R_{BL,n}$ averages internal reflectance over all incident angles on the boundary layer of our anisotropic media. a can be chosen as a length preferably greater than the transport mean free path, but not too much greater to save the calculation time. We choose a = 3.54 μm, which will turn out to be greater than L^*_{zz}. We substitute Eq. (5) into Eq. (2) and linearize the resulting equation as

$$y_2 = \frac{1}{L_{zz}^*}x, \tag{6}$$

where

$$x = L + a\frac{1+\exp(-L/L_{zz})}{T} - 2a \tag{7}$$

and

$$y_2 = -2z_{e0} + K_{zz}\frac{1-\exp(-L/L_{zz})}{T} + z_{e0}\frac{1+\exp(-L/L_{zz})}{T}. \tag{8}$$

We fit the calculated transmittance to Eq. (6) as shown in Fig. 2(b) using z_e = 0.519 obtained from the optical boundary layer theory. In the fit, R^2 is minimized at 0.9917 to yield K_{zz} = 0.9, and we find L^*_{zz} = 2.05 μm from the slope (see Table 1). When the optical boundary layer theory is used for z_e, the coefficient of determination (*i.e.*, goodness of fit) improves over the approximation using z_e = 2/3, increasing the accuracy for L^*_{zz} and K_{zz}.

We have demonstrated that the effective transport mean free path $L^*_{zz}' \equiv K_{zz} L^*_{zz}$, and not L^*_{zz}, should be interpreted as the mean path for randomization of the light propagation direction.[15] The reason is that L^*_{zz}' is related to L_{zz} by

$$L_{zz}^{*\prime} = \frac{L_{zz}}{1-\bar{\mu}(\hat{\mathbf{z}})/K_{zz}}, \tag{9}$$

which satisfies $L^*_{zz}' \geq L_{zz}$, and $L^*_{zz}' = L_{zz}$ at $\bar{\mu}(\hat{\mathbf{z}}) = 0$ where $\bar{\mu}(\hat{\mathbf{z}})$ is the average cosine of scattering polar angles when light is incident in the z direction on the scattering unit. (We will discuss in detail how to determine the scattering unit of *Cyphochilus* scales in Fig. 3.) When z_e is approximately treated as 2/3, the effective transport mean free path is L^*_{zz}' = 1.86 μm from our fit to Eq. (3). In comparison, when the optical boundary layer is used in fitting to Eq. (6), L^*_{zz}' is 1.85 μm, which is only slightly smaller than 1.86 μm (see Table 1). Whereas the accuracy improvement in L^*_{zz}' by the optical boundary layer theory appears small, the accuracy for L^*_{zz}, K_{zz}, and z_e has improved significantly (see

Table 1).

Burresi *et al.* [4] and Cortese *et al.* [5] estimated the transport mean free path of *Cyphochilus* scales in the thickness direction as 1.47 μm and 1.21 μm, respectively. These values were obtained using the isotropic diffusion equation and an approximate z_e calculated based on Fresnel's law for $f = 0.61$. In comparison, our more accurate estimation by the anisotropic diffusion equation and the optical boundary layer theory gives a significantly larger value of $L^*_{zz}' = 1.85$ μm. Because the improvement is due to K_{zz} and z_e, we can estimate more accurate values of the transport mean free path that would have been obtained in refs [4] and [5], if our improved K_{zz} and z_e had been used. For the estimation, we note that Eq. (2) is reduced to

$$T = \frac{1+\left[z_e / K_{zz}\right]}{L / L^*_{zz}'+2\left[z_e / K_{zz}\right]} \tag{10}$$

when the film thickness is sufficiently greater than L_{zz}. In comparison, refs [4] and [5] used

$$T = \frac{1+z_e}{L / l^* + 2z_e}, \tag{11}$$

where $T = 0.30$, $L = 8.1$ μm in ref [4] and $T = 0.29$, $L = 7$ μm in ref [5]. Both refs [4] and [5] used $z_e = 1.63$. Instead of this z_e, when we use our $z_e / K_{zz} = 0.577$ in Eq. (10) with the T and L values in the references, we obtain $L^*_{zz}' = 1.97$ μm and 1.63 μm for refs [4] and [5], respectively. These L^*_{zz}' values are close to our $L^*_{zz}' = 1.85$ μm, whereas the originally obtained transport mean free path values in the references are significantly smaller than our L^*_{zz}'. Note that the experimental measurement of the transport mean free path in the white beetle scales in refs [4] and [5] was performed without removing the solid shell from the scales. The shell would alter z_e and subsequently the calculated transport mean free path values would be affected.

Jacucci *et al.* [8] obtained $L^*_{zz}' = 1.02$ μm by fitting results from anisotropic Monte Carlo simulations to experimentally measured coherent backscattering data. This L^*_{zz}' value is significantly smaller than our result of 1.85 μm and the source of this difference is not trivial to identify. We note that the role of internal reflection in the determination of L^*_{zz}' is intrinsically different between transmittance measurement and coherent backscattering experiment. In the latter experiment,[8] the backscattering signal is mostly from the light that does not penetrate deeply into the structure and can be highly sensitive to the characteristics of internal reflection, which can become complicated for the anisotropic structure. Presumably, the solid shell of the beetle scale and the shell curvature may also have affected the coherent backscattering data.

The good linear fit in Fig. 2(b) indicates that L^*_{zz}' is almost independent of L within our range of L from 0.39 to 4.20 μm ($L / L^*_{zz}' = 0.21 – 2.27$). *In this range, the minimum thickness (0.39 μm) of the simulation volume is even smaller than the effective transport mean free path.* At such small thicknesses, one may find it surprising that L^*_{zz}' is independent of L. Indeed, it is a common belief that the diffusion theory is valid for thicknesses greater than transport mean free path by at least a few times.[18,27-29] When L is too small as in our case, it has been shown that diffusivity D, which is proportional to l^*, would decrease as L decreases.[18] However, the thickness limit for the diffusion theory to be valid may vary widely depending on the nature of scattering[27-29] and the refractive index contrast between the scattering and surrounding media. In general, the thickness limit is lowered as the index contrast decreases.[18,19] For example, for an ideal case of isotropic scattering without the index contrast, Monte Carlo simulation results showed that l^* is almost exactly constant when L is even

down to $0.001l^*$.[24] Our case is similar to this ideal case because L_{zz} (1.78 μm) ≈ L^*_{zz}' (1.85 μm) as in isotropic scattering and the index contrast is absent.

A conventional thought is that a scattering unit cannot be clearly defined in a continuous fibrillar network,[4,6] such as the structure found in white beetle scales, even though the diffusion equation assumes scattering units. Countering this conventional thought, we show that the scattering unit thickness can be clearly defined in the white beetle scale structure for the incident light in the *z*-direction. To determine the scattering unit thickness L_{su} of our structure, we note that the average cosine of polar angles into which light is scattered from a scattering unit is a well-defined quantity. We derived an expression for the average cosine for the light incident in the *z* direction on a scattering unit as[15]

$$\bar{\mu}(\hat{\mathbf{z}}) = K_{zz} - \frac{L_{zz}}{L^*_{zz}}. \tag{12}$$

From Eq. (12), we calculate that $\bar{\mu}(\hat{\mathbf{z}})$ = 0.038. We also define $<\cos\theta>(\hat{\mathbf{z}})$ as average cosine of scattering angles from a simulation volume, when the light is incident in the *z*-direction. Here, when $\bar{\mu}(\hat{\mathbf{z}})$ is same as $<\cos\theta>(\hat{\mathbf{z}})$, the simulation volume thickness can be defined as the scattering unit thickness, *i.e.*, $<\cos\theta>_{L_{su}} = \bar{\mu}$. We calculate $<\cos\theta>$ for varying thickness L of the simulation volume, and the results are given in Fig. 3. From a quadratic regression on the calculated $<\cos\theta>$, we find that $<\cos\theta>$ = 0.038 at L = 3.56 μm, which is the scattering unit thickness L_{su} and, incidentally, twice L_{zz}.

Because $\bar{\mu}(\hat{\mathbf{z}}) / K_{zz}$ is only 0.042 in Eq. (9), L_{zz} (1.78 μm) and L^*_{zz}' (1.85 μm) are close to each other with a less than 4% difference. The close proximity between L_{zz} and L^*_{zz}' is remarkable, because it implies that the light propagation direction is almost perfectly randomized after a single scattering event for the light incident in the *z* direction. To see scattering characteristics for all incident directions, we display in Fig. 4(a) our calculation results for the relation between the cosine of the incident polar angle (θ') and the average cosine of the scattering polar angle (θ) for a scattering unit of the *Cyphochilus* scale. The error bars are determined from different incident azimuthal angles. The small error bars indicate that $<\cos\theta>_{L_{su}}$ is almost independent of azimuthal angles, which is consistent with the rotational symmetry of the structure shown in Fig. 1(a). Figure 4(a) shows a striking optical characteristic that light is scattered backward ($<\cos\theta>_{L_{su}} < 0$) for most of the incident angles from a scattering unit, whose thickness is only $2L_{zz}$. This implies that diffusely incident light is scattered backward on the average. The minimum $<\cos\theta>_{L_{su}}$ is –0.219 at $\cos\theta'$ = 0.1. In ref [15], we noted that, if $<\cos\theta>_{L_{su}}$ is small enough so that it can be even negative, L^*_{zz} can become even smaller than L_{zz}. We see in Fig. 4(a) that negative $<\cos\theta>_{L_{su}}$ is realized. From the negative $<\cos\theta>_{L_{su}}$, we can anticipate that $L^*_{zz} < L_{zz}$, indicating exceptional light scattering. However, we discover that $L^*_{zz} > L_{zz}$ in *Cyphochilus* scales, and this outcome suggests that the beetle scale structure can be further optimized to minimize L^*_{zz}' if K_{zz} could remain the same or decrease.

To see more clearly how light is scattered by the scattering unit, we calculate the fraction of the incident light that is scattered into 45° ≤ θ ≤ 135°, as a function of $\cos\theta'$, as displayed in Fig. 4(b). This fraction, α, represents the tendency of light to be scattered toward lateral directions. For isotropic scattering, α becomes $1/\sqrt{2}$ = 0.707, which is equal to the solid angle fraction for 45° ≤ θ ≤ 135°. For normally incident light, α for the scattering in the *Cyphochilus* scale is very close to that for isotropic scattering. However, for oblique incidences where $\cos\theta' \le 0.6$, the scattering is preferentially toward

lateral directions. The fraction of the light power scattered sideways, when averaged over all incident angles, is equal to $\int_0^1 \alpha \, d(\cos\theta')$. We note in Fig. 4(b) that $\int_0^1 \alpha \, d(\cos\theta') > 1/\sqrt{2}$ is satisfied in the *Cyphochilus* scale. Therefore, this inequality demonstrates that the scattering is preferentially toward lateral directions for diffusely incident light with isotropic intensity.

IV. CONCLUSION

In summary, we have performed detailed characterization on light scattering in *Cyphochilus* white beetle scales by applying the anisotropic diffusion theory to their nanostructures revealed by high-resolution X-ray tomography.[6] Specifically, we have calculated the thickness direction component of anisotropy tensor and scattering / transport mean free path tensors, the average scattering angle, and the extrapolation length ratio of the nanostructures with improved accuracy over previous studies.[4-8] For accurate characterization, we use our optical boundary layer theory and take the anisotropy tensor into account. Our results reveal a striking effect that, within the thickness of only two scattering events ($2L_{zz}$) in the *Cyphochilus* scales, diffusely incident light is scattered backward on the average, with preferential scattering directions being sideways. For normal incidence, the forward and backward scattering probabilities are almost the same as in isotropic scattering, so that the scattering mean free path and the effective transport mean free path, both in the scale thickness direction, are very close to each other with a < 4% difference.

ACKNOWLEDGMENTS

S.E.H. and S.M.H. acknowledge the financial support from the National Science Foundation (NSF) CAREER Award (DMR-1555290) and NSF SEPTET (CHE-1231046), respectively.

REFERENCES

1. D. S. Wiersma, "Disordered photonics," Nat. Photonics **7**, 188-196 (2013).
2. P. Roach, N. J. Shirtcliffe, and M. I. Newton, "Progess in superhydrophobic surface development," Soft Matter **4**, 224-240 (2008).
3. L. J. Gibson and M. F. Ashby, *Cellular solids: Structure and properties* (Cambridge University Press, 1999).
4. M. Burresi, L. Cortese, L. Pattelli, M. Kolle, P. Vukusic, D. S. Wiersma, U. Steiner, and S. Vignolini, "Bright-white beetle scales optimise multiple scattering of light," Sci. Rep. **4**, 6075 (2014).
5. L. Cortese, L. Pattelli, F. Utel, S. Vignolini, M. Burresi, and D. S. Wiersma, "Anisotropic light transport in white beetle scales," Adv. Opt. Mater. **3**, 1337-1341 (2015).
6. B. D. Wilts, X. Sheng, M. Holler, A. Diaz, M. Guizar-Sicairos, J. Raabe, R. Hoppe, S. H. Liu, R. Langford, and O. D. Onelli, "Evolutionary-optimized photonic network structure in white beetle wing scales," Adv. Mater. **30**, 1702057 (2018).
7. P. Vukusic, B. Hallam, and J. Noyes, "Brilliant whiteness in ultrathin beetle scales," Science **315**, 348-348 (2007).
8. G. Jacucci, O. D. Onelli, A. D. Luca, J. Bertolotti, R. Sapienza, and S. Vignolini, "Coherent backscattering of light by an anisotropic biological network," Interface Focus **9**, 20180050 (2018).
9. S. L. Burg, A. Washington, D. M. Coles, A. Bianco, D. McLoughlin, O. O. Mykhaylyk, J. Villanova, A. J. C. Dennison, C. J. Hill, P. Vukusic, S. Doak, S. J. Martin, M. Hutchings, S. R. Parnell, C. Vasilev, N. Clarke, A. J. Ryan, W. Furnass, M. Croucher, R. M. Dalgliesh, S. Prevost, R. Dattani, A. Parker, R. A. L. Jones, J. P. A. Fairclough, and A. J. Parnell, "Liquid–liquid phase separation morphologies in ultra-white beetle scales and a synthetic equivalent," Commun. Chem. **2**, 100 (2019).
10. F. Utel, L. Cortese, D. S. Wiersma, and L. Pattelli, "Optimized white reflectance in photonic-network structures," Adv. Opt. Mater. **7**, 1900043 (2019).
11. G. Jacucci, J. Bertolotti, and S. Vignolini, "Role of anisotropy and refractive index in scattering and whiteness optimization," Adv. Opt. Mater. **7**, 1900980 (2019).
12. P. Vukusic, J. R. Sambles, C. R. Lawrence, and R. J. Wootton, "Quantified interference and diffraction in single morpho butterfly scales," Proc. R. Soc. B **266**, 1403-1411 (1999).
13. H. L. Leertouwer, B. D. Wilts, and D. G. Stavenga, "Refractive index and dispersion of butterfly chitin and bird keratin measured by polarizing interference microscopy," Opt. Express **19**, 24061-24066 (2011).
14. B. T. Hallam, A. G. Hiorns, and P. Vukusic, "Developing optical efficiency through optimized coating structure: Biomimetic inspiration from white beetles," Appl. Opt. **48**, 3243-3249 (2009).
15. S. E. Han, "Transport mean free path tensor and anisotropy tensor in anisotropic diffusion equation," (submitted).
16. S. E. Han, S. Atiganyanun, S. H. Lee, S. Cheek, and S. M. Han, "Determination of internal reflectance for photonic glasses," Phys. Rev. B **99**, 054206 (2019).
17. S. Torquato, *Random heterogeneous materials: Microstructure and macroscopic properties* (Springer, 2002).
18. R. Elaloufi, R. Carminati, and J.-J. Greffet, "Diffusive-to-ballistic transition in dynamic light transmission through thin scattering slabs: A radiative transfer approach," J. Opt. Soc. Am. A **21**, 1430-1437 (2004).
19. L. Pattelli, G. Mazzamuto, D. S. Wiersma, and C. Toninelli, "Diffusive light transport in semitransparent media," Phys. Rev. A **94**, 043846 (2016).
20. K. Busch, C. M. Soukoulis, and E. N. Economou, "Transport and scattering mean free paths of classical waves," Phys. Rev. B **50**, 93-98 (1994).
21. C. M. Soukoulis, S. Datta, and E. N. Economou, "Propagation of classical waves in random media," Phys. Rev. B **49**, 3800-3810 (1994).
22. S. Atiganyanun, J. B. Plumley, S. J. Han, K. Hsu, J. Cytrynbaum, T. L. Peng, S. M. Han, and S. E. Han, "Effective radiative cooling by paint-format microsphere-based photonic random media," ACS Photon. **5**, 1181-1187 (2018).
23. C. F. Bohren and D. R. Huffman, *Absorption and scattering of light by small particles* (John Wiley & Sons, 1983).
24. D. J. Durian, "Influence of boundary reflection and refraction on diffusive photon transport," Phys. Rev. E **50**, 857-866 (1994).
25. J. X. Zhu, D. J. Pine, and D. A. Weitz, "Internal reflection of diffusive light in random media," Phys. Rev. A **44**, 3948-3959 (1991).
26. E. Alerstam, "Anisotropic diffusive transport: Connecting microscopic scattering and macroscopic transport properties," Phys. Rev. E **89**, 063202 (2014).
27. R. H. J. Kop, P. de Vries, R. Sprik, and A. Lagendijk, "Observation of anomalous transport of strongly multiple scattered light in thin disordered slabs," Phys. Rev. Lett. **79**, 4369-4372 (1997).
28. X. Zhang and Z.-Q. Zhang, "Wave transport through thin slabs of random media with internal reflection: Ballistic to diffusive transition," Phys. Rev. E **66**, 016612 (2002).
29. I. M. Vellekoop, P. Lodahl, and A. Lagendijk, "Determination of the diffusion constant using phase-sensitive measurements," Phys. Rev. E **71**, 056604 (2005).

Figures

Fig. 1. (a-c) Two-point probability function S_2 of *Cyphochilus* white beetle scales in (a) *xy*-plane, (b) *xz*-plane, and (c) along the 3 principal directions. (d,e) Black-and-white X-ray tomography images in the *xy*-plane of the scales (d) in the middle and (e) near the boundary along the thickness direction. (f) Electron micrograph in an *xz*-plane of the scales exposed by a focused ion beam and (g) black-and-white version of the same image.

Fig. 2. (a) Plot of $\log(1/T_b)$ vs. L, where the inverse slope is L_{zz}. (b) Plot of y_2 vs. x defined in Eqs. (7) and (8), where the inverse slope is L^*_{zz}. In both (a) and (b), symbols represent optical simulations and dashed line is a linear regression on the simulation results. Images in the middle of (a) and (b) are the *Cyphochilus* white beetle scales used in the simulations.

Fig. 3. Plot of $< \cos\theta > (\hat{\mathbf{z}})$ as function of L to determine the scattering unit thickness L_{su} = 3.56 μm.

Fig. 4. (a) Mean cosine of the scattering angle $< \cos\theta >_{L_{su}}$ and (b) fraction of scattering toward lateral directions α as a function of cosine of the incident angle θ' for a scattering unit of *Cyphochilus* white beetle scales. Inset shows the definition of θ and θ'.

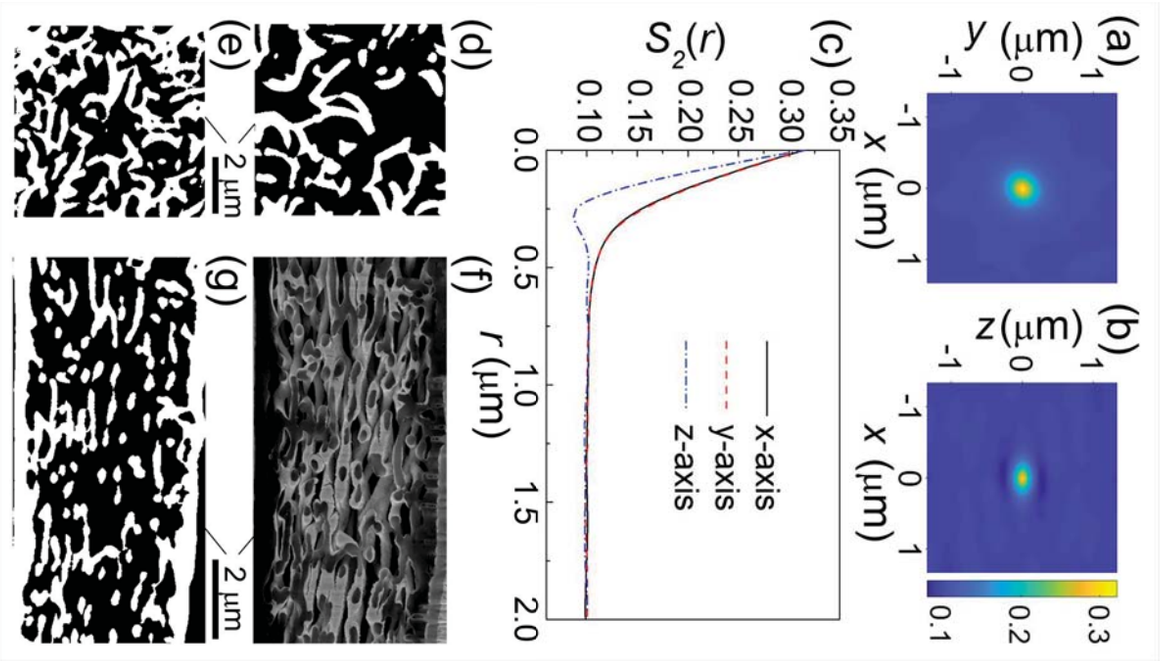

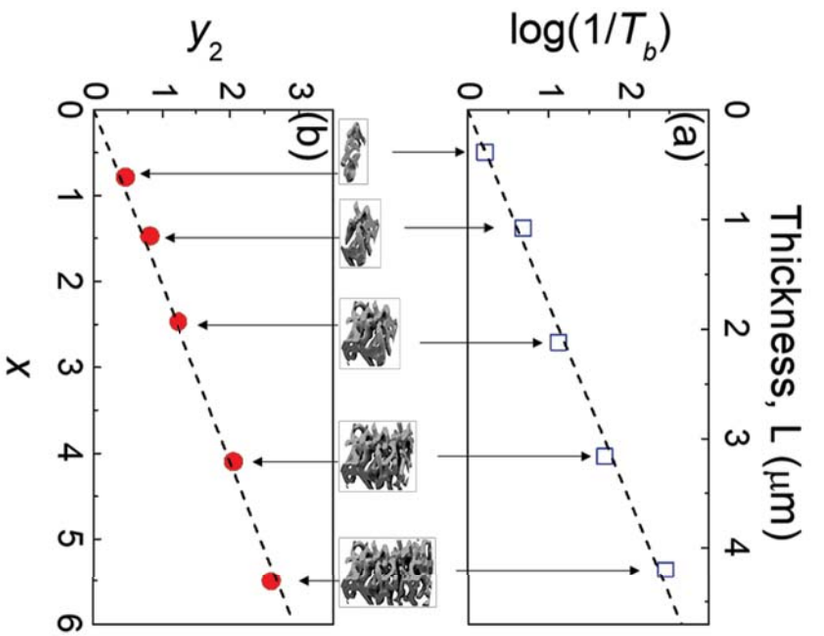

PLEASE CITE THIS ARTICLE AS DOI: 10.1063/1.5144688

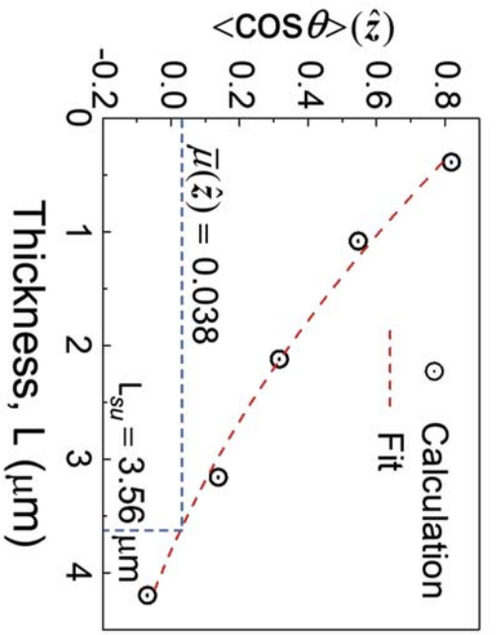

PLEASE CITE THIS ARTICLE AS DOI: 10.1063/1.5144688